Electron Trapping Mechanism in $LaAlO_3/SrTiO_3$ Heterostructures

Chunhai Yin,[1] Alexander E. M. Smink,[2] Inge Leermakers,[3] Lucas M. K. Tang,[3] Nikita Lebedev,[1] Uli Zeitler,[3] Wilfred G. van der Wiel,[2] Hans Hilgenkamp,[2] and Jan Aarts[1]

[1]*Huygens-Kamerlingh Onnes Laboratory, Leiden University, P.O. Box 9504, 2300 RA Leiden, The Netherlands*

[2]*MESA+ Institute for Nanotechnology, University of Twente, P.O. Box 217, 7500 AE Enschede, The Netherlands*

[3]*High Field Magnet Laboratory (HFML-EMFL), Radboud University, Toernooiveld 7, 6525 ED Nijmegen, The Netherlands*

(Received 24 February 2019; revised manuscript received 13 September 2019; published 7 January 2020)

In $LaAlO_3/SrTiO_3$ heterostructures, a still poorly understood phenomenon is that of electron trapping in back-gating experiments. Here, by combining magnetotransport measurements and self-consistent Schrödinger-Poisson calculations, we obtain an empirical relation between the amount of trapped electrons and the gate voltage. The amount of trapped electrons decays exponentially away from the interface. However, contrary to earlier observations, we find that the Fermi level remains well within the quantum well. The enhanced trapping of electrons induced by the gate voltage can therefore not be explained by a thermal escape mechanism. Further gate sweeping experiments strengthen that conclusion. We propose a new mechanism which involves the electromigration and clustering of oxygen vacancies in $SrTiO_3$ and argue that such electron trapping is a universal phenomenon in $SrTiO_3$-based two-dimensional electron systems.

DOI: 10.1103/PhysRevLett.124.017702

Controlling the electronic properties of materials by applying an external voltage is at the heart of modern electronics. This is also true for oxide heterostructures, where the quasi-two-dimensional electron gas (Q2DEG) discovered at the interface between $LaAlO_3$ (LAO) and $SrTiO_3$ (STO) [1] displays a multitude of physical properties, such as superconductivity [2], signatures of magnetism [3–5] and even their coexistence [6,7]. Due to the large permittivity of the STO substrate [8], the carrier density and mobility of the Q2DEG can be modulated by a back-gate voltage (V_G). Gate-tunable insulator to metal transitions [9], insulator to superconductor transitions [10] and Rashba spin-orbit interactions [11,12] have been reported. At the LAO/STO interface, the Q2DEG is confined in a quantum well (QW) on the STO side and the band structure is formed by the Ti t_{2g} orbitals. For LAO films grown on STO (001) substrates, the d_{xy} band lies below the $d_{xz,yz}$ bands in energy [13–15]. Applying V_G across the STO substrate changes the carrier density in the QW. A Lifshitz transition occurs when the Fermi level is tuned across the bottom of the $d_{xz,yz}$ bands [16]. In back-gating experiments, a commonly observed phenomenon is that the sheet resistance (R_s) follows an irreversible route when V_G is swept first forward and then backward [10,17–20]. The explanation given by Biscaras *et al.* [18] is that the Fermi level lies intrinsically close to the top of the QW. High-mobility electrons escape and get trapped in STO when the carrier density is beyond a threshold. But the relations between the amount of trapped electrons, their spatial distribution, and the gate voltage are still unknown. We study these relations by combining magnetotransport measurements and self-consistent Schrödinger-Poisson calculations on samples grown by sputtering and pulsed laser deposition (PLD). In both cases, the thermal escape mechanism cannot be reconciled with our results. Further gate sweeping experiments strengthen this conclusion. We propose a new mechanism which involves the electromigration and clustering of oxygen vacancies in $SrTiO_3$. Results of the sputtered sample are discussed in the main text, those of the PLD-grown sample are in the Supplemental Material [21].

Hall bar devices were used as depicted in Fig. 1(a) (inset), of length 1000 μm and width 150 μm. First, a sputtered amorphous AlO_x hard mask in the form of a negative Hall bar geometry (thickness ~15 nm) was fabricated on a TiO_2-terminated STO (001) substrate [26] by photolithography. Then, 15 unit cells of LAO film were deposited at 800 °C in an Ar pressure of 0.04 mbar by 90° off-axis sputtering [27]. Finally, the sample was *in situ* annealed at 600 °C in 1 mbar of oxygen for 1 h. The backgate electrode was formed by uniformly applying a thin silver paint layer (Ted Pella, Inc.) on the back of the substrate. Device fabrication details are described in the Supplemental Material [21]. The longitudinal and transverse resistances (R_{xx}, R_{xy}) were measured simultaneously by standard lock-in technique ($f = 13.53$ Hz and $i_{\mathrm{RMS}} = 1.0$ μA). Magnetotransport measurements were performed under different V_G at 4.2 K in a superconducting magnet (field sweep ± 15 T). The maximum applied V_G was +200 V. The leakage current was less than 1 nA during the measurement.

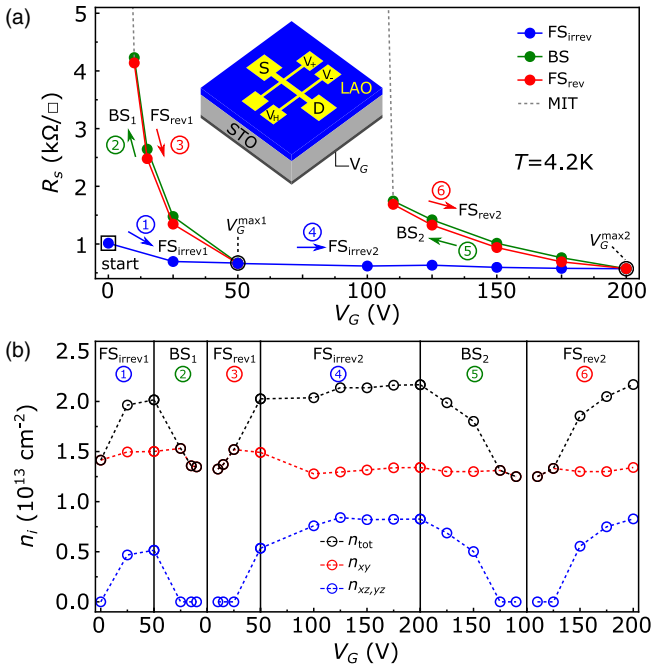

FIG. 1. (a) V_G dependence of sheet resistance (R_s) at 4.2 K. The solid circles are $R_s(B=0)$ in magnetoresistance curves. The blue, green, and red arrows indicate the irreversible forward sweep (FS$_{irrev}$), backward sweep (BS), and reversible forward sweep (FS$_{rev}$), respectively. The sweep order is indicated by the circled numbers. Two BSs were performed at 50 V ($V_G^{max\,1}$) and 200 V ($V_G^{max\,2}$). The gray dashed line indicates the metal-insulator transition (MIT). The inset shows a schematic of the Hall bar device. Source and drain are labeled as S and D. The longitudinal resistance (R_{xx}) is measured between V_+ and V_- and the transverse resistance (R_{xy}) between V_H and V_-. V_G is applied between the back of the substrate and the drain. (b) V_G dependence of the carrier density in different regimes. The red and blue circles represent the carrier density of the d_{xy} band (n_{xy}) and $d_{xz,yz}$ band ($n_{xz,yz}$). The black circles are the total carrier density (n_{tot}) which is the sum of n_{xy} and $n_{xz,yz}$.

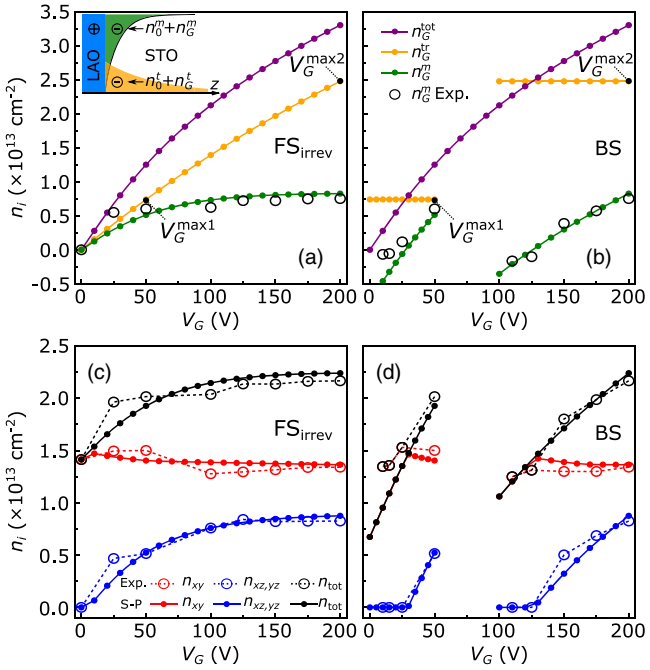

FIG. 2. (a), (b) V_G dependence of the calculated gate-induced total charge density (n_G^{tot}, purple), trapped charge density (n_G^{tr}, yellow), mobile charge density (n_G^m, green) and measured gate-induced mobile charge density (n_G^m Exp., open black circle) in (a) FS$_{irrev}$ and (b) BS regimes. The inset of (a) shows an illustration of the interface for Schrödinger-Poisson calculations. (c), (d) V_G dependence of S-P calculations that are calculated (solid circles) and measured (open circles) n_{xy} (red), $n_{xz,yz}$ (blue), and n_{tot} (black) in (a) FS$_{irrev}$ and (b) BS regimes.

The device was cooled down to 4.2 K with V_G grounded. Figure 1(a) shows the V_G dependence of the sheet resistance, R_s. V_G was first increased from 0–50 V ($V_G^{max\,1}$), resulting in a decrease of R_s. This sweep is called an irreversible forward sweep (FS$_{irrev}$), because R_s increased above the virgin curve when V_G was swept backward. The backward sweep (BS) led to a metal-insulator transition (MIT), which is consistent with earlier reports [19]. After the onset of the MIT, V_G was further decreased to completely deplete the QW. When V_G was swept forward again, R_s followed the same route as the BS. Therefore the latter forward sweep is named a reversible forward sweep (FS$_{rev}$). Another BS was performed at 200 V ($V_G^{max\,2}$). It is seen that R_s increased faster in BS$_1$ than in BS$_2$, a point to be discussed later. We also applied negative voltages. Those sweeps are always reversible, as discussed in the Supplemental Material [21].

Figure 1(b) shows the V_G dependence of the carrier density of both d_{xy} (n_{xy}) and $d_{xz,yz}$ ($n_{xz,yz}$) bands and the total carrier density (n_{tot}). The values were extracted by fitting the magnetotransport data with a two-band model [15,21]. It can be seen that only the d_{xy} band was occupied at 0 V. In FS$_{irrev1}$, electrons were added into the QW and the Lifshitz transition occurred at a carrier density (n_L) of 1.51×10^{13} cm^{-2}, which is close to earlier reported values [16]. In BS$_1$, n_{tot} decreased to 1.33×10^{13} cm^{-2} at 10 V, which is the onset of the MIT, comparable to the earlier reported carrier density (0.5–1.5 $\times 10^{13}$ cm^{-2}) for the MIT [28]. In FS$_{rev1}$, the carrier densities of the bands were tuned reversibly as in BS$_1$ and the system was fully recovered when 50 V was reapplied. In FS$_{irrev2}$, n_{tot} saturated at 2.17×10^{13} cm^{-2} beyond 125 V. In BS$_2$, the MIT occurred at 110 V with a carrier density of 1.25×10^{13} cm^{-2}, which could be due to the Hall bar contacts becoming insulating faster than the channel [29]. A noteworthy feature is that the amount of gate-induced trapped electrons is independent of the number of backward sweeps and is only related to V_G^{max}.

First, we study the relation between the amount of trapped electrons and the gate voltage. In a backgating experiment, the total amount of electrons (n_G^{tot}) induced by V_G, as shown by the purple curves in Figs. 2(a) and 2(b),

can be calculated using a parallel plate capacitor model [30,31]:

$$n_G^{\mathrm{tot}}(V_G) = \int_{V_1}^{V_2} \frac{\epsilon_0}{e d_{\mathrm{STO}}} \epsilon_r(V_G) dV_G, \tag{1}$$

where ϵ_0 is the vacuum permittivity, e is the electron charge and d_{STO} is the thickness of the STO substrate (0.5 mm). The field-dependent permittivity of the STO substrate $\epsilon_r(V_G)$ is calculated following Ref. [32]:

$$\epsilon_r(E) = 1 + \frac{B}{[1 + (E/E_0)^2]^{1/3}}, \tag{2}$$

where the electric field $E = V_G/d_{\mathrm{STO}}$, $B = 2.55 \times 10^4$ and $E_0 = 8.22 \times 10^4$ V/m. In $\mathrm{FS_{irrev}}$ regimes, as shown in Fig. 2(a), a part of n_G^{tot} becomes gate-induced trapped electrons (n_G^{tr}) in STO. Subtracting n_G^{tr} from n_G^{tot} will give the amount of gate-induced mobile electrons (n_G^m) which are doped into the QW. We find that the relation between n_G^{tr} and V_G can be described using the following expression:

$$n_G^{\mathrm{tr}}(V_G) = N(1 - e^{-V_G/400}), \tag{3}$$

which yields the yellow curve, where $N = 6.2 \times 10^{13}$ cm^{-2}. The subtraction ($n_G^{\mathrm{tot}} - n_G^{\mathrm{tr}} = n_G^m$) is given by the green curve, and gives a good description of the measured n_G^m (open black circle). In BS regimes, as shown in Fig. 2(b), n_G^{tot} is given by V_G according to Eq. (1). However, the value of n_G^{tr} is fixed at the $n_G^{\mathrm{tr}}(V_G^{\max})$. Thus, n_G^m is smaller than its counterpart in $\mathrm{FS_{irrev}}$ regimes. In both BS regimes the calculated n_G^m is in good agreement with the experimental data. Moreover, due to the field-dependent permittivity, dn_G^{tot}/dV_G is decreasing as V_G increases. As a consequence, the same negative ΔV_G removes more mobile electrons at 50 V rather than at 200 V, which could explain the fact that R_s increases faster in $\mathrm{BS_1}$ than in $\mathrm{BS_2}$. It should be noted that the empirical formula of $n_G^{\mathrm{tr}}(V_G)$ is not universal, but instead varies among samples. We performed similar V_G sweeps on two reference samples and observed slightly different V_G dependence of R_s (see Fig. S5 in the Supplemental Material [21]). Thus, $n_G^{\mathrm{tr}}(V_G)$ should always be obtained from experimental results.

Next, we use the self-consistent Schrödinger-Poisson (S-P) model to study the charge distribution and band occupation [15,33–36]. S-P calculations are based on the effective mass and envelope wave function approximations. Due to the orbital orientation, d_{xy} and $d_{xz,yz}$ orbitals are heavy and light in the z direction, respectively. We take the effective masses as $m_{xy}^{*z} = 14\ m_e$ and $m_{xz,yz}^{*z} = 0.7\ m_e$ [14,15,35], where m_e is the electron mass. We take $z > 0$ to be STO. In the original state, there are initial mobile electrons (n_0^m, 1.41×10^{13} cm^{-2} in our sample) and initial trapped electrons (n_0^{tr}) on the STO side, and an equivalent amount of positive charges on the LAO side to keep overall charge neutrality.

The spatial distributions of the trapped electrons, both n_0^{tr} and $n_G^{\mathrm{tr}}(V_G)$, are input parameters of the S-P model, which effectively influence the V_G dependent occupation of the d_{xy} and $d_{xz,yz}$ bands. In our calculations, we obtain the best results by using the following distribution of the trapped electrons:

$$n_{3\mathrm{D}}^{\mathrm{tr}}(z, V_G) = \begin{cases} 0 & \text{for } z < 0 \\ \frac{n_0^{\mathrm{tr}} + n_G^{\mathrm{tr}}(V_G)}{\lambda} e^{-z/\lambda} & \text{for } z \geq 0 \end{cases} \tag{4}$$

where $n_0^{\mathrm{tr}} = 6.4 \times 10^{13}$ cm^{-2} and $\lambda = 50$ nm. The integration range is from 0 to 100 nm, which is divided into 2000 equal sections. The calculated evolutions of n_{xy} and $n_{xz,yz}$ in $\mathrm{FS_{irrev}}$ and BS regimes are shown in Figs. 2(c) and 2(d), closely agreeing with the experimental data.

Based on the above analysis, we could obtain the confining potential profile, the Fermi energy and the spatial distribution of mobile electrons occupying the d_{xy} and $d_{xz,yz}$ bands. Figures 3(a)–3(c) show the results at 0, 50, and 200 V, respectively. The mobile electrons are confined within ~10 nm at the interface, which agrees with the reported spatial distribution of the Q2DEG [37–39]. Figure 3(d) shows the confining potential in a larger range. In all cases the Fermi level is well below the top of the QW; therefore the probability of mobile electrons thermally escaping [$k_B T(4.2\ \mathrm{K}) \approx 0.36$ meV] from the QW should be very low. The subband dispersions of the three cases are shown in Figs. 3(e)–3(g). We note that increasing V_G decreases the spacing between the subband levels.

In order to check the thermal escape mechanism [18] in more detail, we warmed the device to room temperature to remove the trapping [17], cooled down again to 4.2 K and performed multiple backward sweeps from 10 to 50 V. As shown in Fig. 4, a growing R_s separation between $\mathrm{FS_{irrev}}$ and BS is seen as $V_G^{\max}$ increases. In the thermal escape mechanism, electron trapping only occurs after R_s (or n_{tot}) reaches its saturation. However, our experiment clearly shows that trapping occurs immediately when positive V_G is applied and the amount of trapped electrons increases as $V_G^{\max}$ increases. So we can rule out thermal escaping of mobile electrons to be the mechanism for electron trapping. We performed the same magnetotransport measurements and S-P calculations on a PLD-grown sample. Although the characteristic transport and fitting parameters of the PLD sample were very different from the sputtered one, the Fermi level was also found to stay well within the quantum well. Moreover, similar irreversible behavior has been reported in other Q2DEG systems, such as $\mathrm{LaTiO_3/STO}$ [18], $\mathrm{LaVO_3/STO}$ [20], $(\mathrm{LaAlO_3})_{0.3}(\mathrm{Sr_2AlTaO_6})_{0.7}/\mathrm{STO}$ [40], and amorphous LAO/STO [41]. Therefore the electron trapping phenomenon appears intrinsic to the STO substrate. We also checked whether the structural

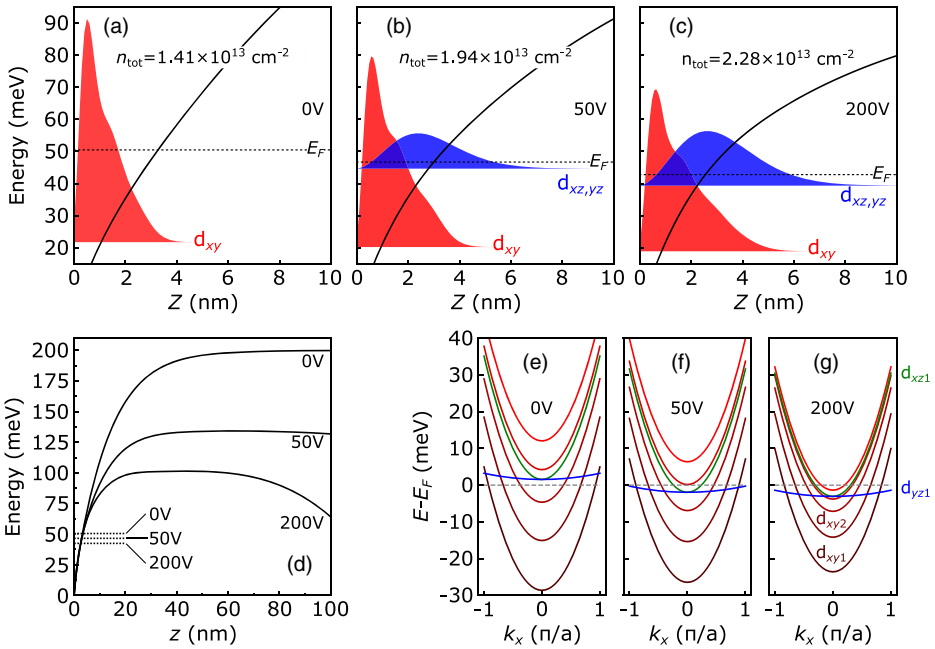

FIG. 3. (a)–(c) S-P calculations confining potential profile (solid line), Fermi energy (dotted line), and spatial distribution of mobile electrons occupying d_{xy} (red) and $d_{xz,yz}$ (blue) bands at (a) 0, (b) 50, and (c) 200 V. (d) Confining potential and Fermi energy in a larger range. (e), (f) S-P calculated subband dispersions in parabolic approximation at (e) 0, (f) 50, and (g) 200 V.

phase transition of the STO substrate at 105 K plays a role in the trapping [42–44]. Gating experiments at 4, 80, and 120 K all showed hysteresis, as shown in the Supplemental Material [21]. We conclude that tetragonal domain formation is not important for what we observe.

We propose a two-step trapping mechanism involving redistribution of oxygen vacancies (V_O's) in STO under influence of an electric field. The first step is the electromigration of V_O's. Among all types of defects in STO, V_O has the lowest activation enthalpy for migration [45] as reported in previous works [46–48]. The second step is the clustering of V_O's which could form in-gap trapping states [49,50], of which the energy was recently determined to be ~0.31 and ~1.11 eV below the conduction band [51]. Figure 5 shows the dynamic resistance change during and after V_G sweeps in the FS_{irrev} and BS regimes. The electron trapping mechanism can then be explained as follows. In FS_{irrev} regimes as shown in Fig. 5(a), the effect of

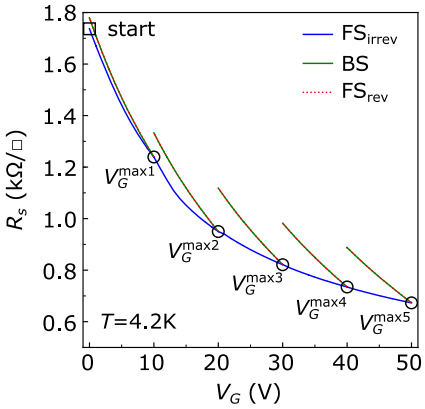

FIG. 4. V_G dependence of R_s at 4.2 K. The sweep order is similar to that in Fig. 1(a). Backward sweeps were performed from 10 to 50 V. Note that BS and FS_{rev} overlap perfectly.

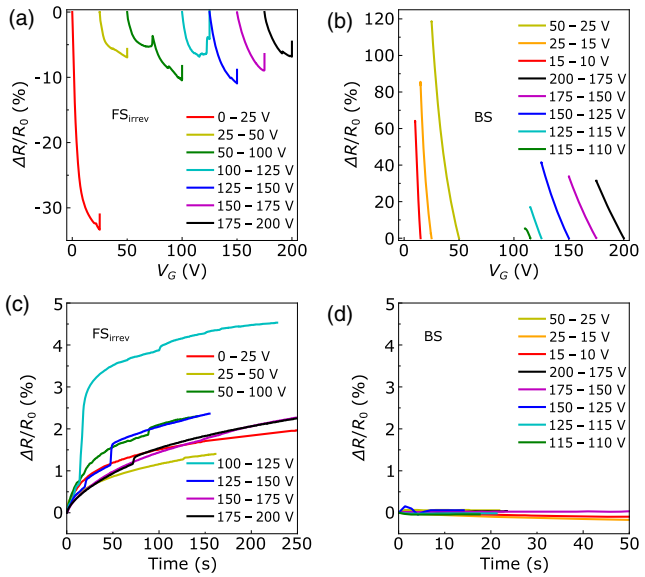

FIG. 5. (a), (b) Dynamic change of R_s during V_G sweeps in (a) FS_{irrev} and (b) BS regimes. V_G was swept at a rate of 0.1 V/s. R_s measurements kept on going for several minutes after the stabilization of V_G. (c), (d) Dynamic change of R_s after V_G sweeps in (c) FS_{irrev} and (d) BS regimes.

increasing V_G is twofold. One is to add electrons into the QW. The other is to push positively charged V_O's migrating toward the interface. The clustering of the accumulated V_O's then forms in-gap trapping states. Several sudden resistance jumps can be clearly seen during V_G sweeps, which might be due to the formation of big V_O clusters. Moreover, after stabilizing the gate voltage as shown in Fig. 5(c), the electromigration and clustering of V_O's do not stop immediately. Newly formed in-gap states still trap conduction electrons, resulting in an immediate increase of R_s when V_G stabilizes. In BS and FS_{rev} regimes as shown in Figs. 5(b) and 5(d), sweeping V_G only changes the carrier density in the QW without modifying the defect landscape near the interface. Therefore the system can be tuned in a reversible manner. A schematic illustration of our proposed electric field-driven trapping mechanism is shown in the Supplemental Material [21].

Summarizing, we studied electron trapping in LAO/STO heterostructures under backgate voltages. Combined magnetrotransport measurements and self-consistent Schrödinger-Poisson calculations yield a relation between the amount of trapped electrons and the gate voltage as well as the spatial distribution of the trapped electrons. We propose a new trapping mechanism which involves the electromigration and clustering of oxygen vacancies in STO, since our analysis shows that the thermal escape mechanism is not valid. This is relevant for theoretical works [35,52,53], where the assumption was that all the gate-induced electrons land in the QW. We obtained qualitatively similar results from the samples grown by sputtering and PLD, and conclude that electron trapping is a universal phenomenon in $SrTiO_3$-based two-dimensional electron systems.

We thank Nicandro Bovenzi, Andrea Caviglia, Stefano Gariglio, Haijiao Harsan Ma, Yulin Gan, Felix Gunkel, Kevin Steffen, Prateek Kumar, and Aymen Ben Hamida for discussions and Anatolie Mitioglu and Lisa Rossi for technical assistance. This work is supported by the Netherlands Organisation for Scientific Research (NWO) through the DESCO program. We acknowledge the support of HFML-RU/NWO, member of the European Magnetic Field Laboratory (EMFL). C. Y. is supported by China Scholarship Council (CSC) with Grant No. 201508110214.

[1] A. Ohtomo and H. Y. Hwang, Nature (London) **427**, 423 (2004).
[2] N. Reyren, S. Thiel, A. D. Caviglia, L. F. Kourkoutis, G. Hammerl, C. Richter, C. W. Schneider, T. Kopp, A.-S. Ruetschi, D. Jaccard, M. Gabay, D. A. Muller, J.-M. Triscone, and J. Mannhart, Science **317**, 1196 (2007).
[3] A. Brinkman, M. Huijben, M. V. Zalk, J. Huijben, U. Zeitler, J. C. Maan, W. G. V. D. Wiel, G. Rijnders, D. H. A. Blank, and H. Hilgenkamp, Nat. Mater. **6**, 493 (2007).
[4] Ariando, X. Wang, G. Baskaran, Z. Q. Liu, J. Huijben, J. B. Yi, A. Annadi, A. R. Barman, A. Rusydi, S. Dhar, Y. P. Feng, J. Ding, H. Hilgenkamp, and T. Venkatesan, Nat. Commun. **2**, 188 (2011).
[5] J.-S. Lee, Y. W. Xie, H. K. Sato, C. Bell, Y. Hikita, H. Y. Hwang, and C.-C. Kao, Nat. Mater. **12**, 703 (2013).
[6] L. Li, C. Richter, J. Mannhart, and R. C. Ashoori, Nat. Phys. **7**, 762 (2011).
[7] J. A. Bert, B. Kalisky, C. Bell, M. Kim, Y. Hikita, H. Y. Hwang, and K. A. Moler, Nat. Phys. **7**, 767 (2011).
[8] R. C. Neville, B. Hoeneisen, and C. A. Mead, J. Appl. Phys. **43**, 2124 (1972).
[9] S. Thiel, G. Hammerl, A. Schmehl, C. W. Schneider, and J. Mannhart, Science **313**, 1942 (2006).
[10] A. D. Caviglia, S. Gariglio, N. Reyren, D. Jaccard, T. Schneider, M. Gabay, S. Thiel, G. Hammerl, J. Mannhart, and J.-M. Triscone, Nature (London) **456**, 624 (2008).
[11] M. Ben Shalom, M. Sachs, D. Rakhmilevitch, A. Palevski, and Y. Dagan, Phys. Rev. Lett. **104**, 126802 (2010).
[12] A. D. Caviglia, M. Gabay, S. Gariglio, N. Reyren, C. Cancellieri, and J.-M. Triscone, Phys. Rev. Lett. **104**, 126803 (2010).
[13] M. Salluzzo, J. C. Cezar, N. B. Brookes, V. Bisogni, G. M. De Luca, C. Richter, S. Thiel, J. Mannhart, M. Huijben, A. Brinkman, G. Rijnders, and G. Ghiringhelli, Phys. Rev. Lett. **102**, 166804 (2009).
[14] A. F. Santander-Syro, O. Copie, T. Kondo, F. Fortuna, S. Pailhès, R. Weht, X. G. Qiu, F. Bertran, A. Nicolaou, A. Taleb-Ibrahimi, P. Le Fèvre, G. Herranz, M. Bibes, N. Reyren, Y. Apertet, P. Lecoeus, A. Barthélémy, and M. J. Rozenberg, Nature (London) **469**, 189 (2011).
[15] A. E. M. Smink, J. C. de Boer, M. P. Stehno, A. Brinkman, W. G. van der Wiel, and H. Hilgenkamp, Phys. Rev. Lett. **118**, 106401 (2017).
[16] A. Joshua, S. Pecker, J. Ruhman, E. Altman, and S. Ilani, Nat. Commun. **3**, 1129 (2012).
[17] C. Bell, S. Harashima, Y. Kozuka, M. Kim, B. G. Kim, Y. Hikita, and H. Y. Hwang, Phys. Rev. Lett. **103**, 226802 (2009).
[18] J. Biscaras, S. Hurand, C. Feuillet-Palma, A. Rastogi, R. C. Budhani, N. Reyren, E. Lesne, J. Lesueur, and N. Bergeal, Sci. Rep. **4**, 6788 (2015).
[19] W. Liu, S. Gariglio, A. Fête, D. Li, M. Boselli, D. Stornaiuolo, and J.-M. Triscone, APL Mater. **3**, 062805 (2015).
[20] H. Liang, L. Cheng, L. Wei, Z. Luo, G. Yu, C. Zeng, and Z. Zhang, Phys. Rev. B **92**, 075309 (2015).
[21] See Supplemental Material at http://link.aps.org/supplemental/10.1103/PhysRevLett.124.017702 for device fabrication, measurements, two-band model fitting, S-P calculations on sputtered and PLD-grown samples, and a schematic illustration of the trapping mechanism, which includes Refs. [22–25].
[22] N. Banerjee, M. Huijben, G. Koster, and G. Rijnders, Appl. Phys. Lett. **100**, 041601 (2012).
[23] P. D. Eerkes, W. G. van der Wiel, and H. Hilgenkamp, Appl. Phys. Lett. **103**, 201603 (2013).
[24] D. Rakhmilevitch, I. Neder, M. B. Shalom, A. Tsukernik, M. Karpovski, Y. Dagan, and A. Palevski, Phys. Rev. B **87**, 125409 (2013).

[25] C. Richter, H. Boschker, W. Dietsche, E. Fillis-Tsirakis, R. Jany, F. Loder, L. F. Kourkoutis, D. A. Muller, J. R. Kirtley, C. W. Schneider, and J. Mannhart, Nature (London) **502**, 528 (2013).
[26] G. Koster, B. L. Kropman, G. J. H. M. Rijnders, D. H. A. Blank, and H. Rogalla, Appl. Phys. Lett. **73**, 2920 (1998).
[27] C. Yin, D. Krishnan, N. Gauquelin, J. Verbeeck, and J. Aarts, Phys. Rev. Mater. **3**, 034002 (2019).
[28] Y. C. Liao, T. Kopp, C. Richter, A. Rosch, and J. Mannhart, Phys. Rev. B **83**, 075402 (2011).
[29] A. E. M. Smink, M. P. Stehno, J. C. de Boer, A. Brinkman, W. G. van der Wiel, and H. Hilgenkamp, Phys. Rev. B **97**, 245113 (2018).
[30] K. S. Novoselov, A. K. Geim, S. V. Morozov, D. Jiang, Y. Zhang, S. V. Dubonos, I. V. Grigorieva, and A. A. Firsov, Science **306**, 666 (2004).
[31] T. Ihn, *Semiconductor Nanostructures: Quantum States and Electronic Transport* (Oxford University Press, Oxford, 2015).
[32] S. Gariglio, A. Fête, and J.-M. Triscone, J. Phys. Condens. Matter **27**, 283201 (2015).
[33] F. Stern, Phys. Rev. B **5**, 4891 (1972).
[34] J. Biscaras, N. Bergeal, S. Hurand, C. Grossetête, A. Rastogi, R. C. Budhani, D. Le Boeuf, C. Proust, and J. Lesueur, Phys. Rev. Lett. **108**, 247004 (2012).
[35] N. Scopigno, D. Bucheli, S. Caprara, J. Biscaras, N. Bergeal, J. Lesueur, and M. Grilli, Phys. Rev. Lett. **116**, 026804 (2016).
[36] D. Li, S. Lemal, S. Gariglio, Z. Wu, A. Fête, M. Boselli, P. Ghosez, and J.-M. Triscone, Adv. Sci. **5**, 1800242 (2018).
[37] M. Basletic, J.-L. Maurice, C. Carrétéro, G. Herranz, O. Copie, M. Bibes, E. Jacquet, K. Bouzehouane, S. Fusil, and A. Barthélémy, Nat. Mater. **7**, 621 (2008).
[38] M. Sing, G. Berner, K. Goß, A. Müller, A. Ruff, A. Wetscherek, S. Thiel, J. Mannhart, S. A. Pauli, C. W. Schneider, P. R. Willmott, M. Gorgoi, F. Schäfers, and R. Claessen, Phys. Rev. Lett. **102**, 176805 (2009).
[39] N. Reyren, S. Gariglio, A. D. Caviglia, D. Jaccard, T. Schneider, and J.-M. Triscone, Appl. Phys. Lett. **94**, 112506 (2009).
[40] V. V. Bal, Z. Huang, K. Han, Ariando, T. Venkatesan, and V. Chandrasekhar, Appl. Phys. Lett. **111**, 081604 (2017).
[41] A. V. Bjørlig, M. V. Soosten, R. Erlandsen, R. T. Dahm, Y. Zhang, Y. Gan, Y. Chen, N. Pryds, and T. S. Jespersen, Appl. Phys. Lett. **112**, 171606 (2018).
[42] B. Kalisky, E. M. Spanton, H. Noad, J. R. Kirtley, K. C. Nowack, C. Bell, H. K. Sato, M. Hosoda, Y. Xie, Y. Hikita, C. Woltmann, G. Pfanzelt, R. Jany, C. Richter, H. Y. Hwang, J. Mannhart, and K. A. Moler, Nat. Mater. **12**, 1091 (2013).
[43] H. J. Harsan Ma, S. Scharinger, S. W. Zeng, D. Kohlberger, M. Lange, A. Sthr, X. R. Wang, T. Venkatesan, R. Kleiner, J. F. Scott, J. M. D. Coey, D. Koelle, and Ariando, Phys. Rev. Lett. **116**, 257601 (2016).
[44] Y. Frenkel, N. Haham, Y. Shperber, C. Bell, Y. Xie, Z. Chen, Y. Hikita, H. Y. Hwang, E. K. H. Salje, and B. Kalisky, Nat. Mater. **16**, 1203 (2017).
[45] V. Metlenko, A. H. H. Ramadan, F. Gunkel, H. Du, H. Schraknepper, S. Hoffmann-Eifert, R. Dittmann, R. Waser, and R. A. D. Souza, Nanoscale **6**, 12864 (2014).
[46] J. Hanzig, M. Zschornak, F. Hanzig, E. Mehner, H. Stöcker, B. Abendroth, C. Röder, A. Talkenberger, G. Schreiber, D. Rafaja, S. Gemming, and D. C. Meyer, Phys. Rev. B **88**, 024104 (2013).
[47] Y. Lei, Y. Li, Y. Z. Chen, Y. W. Xie, Y. S. Chen, S. H. Wang, J. Wang, B. G. Shen, N. Pryds, H. Y. Hwang, and J. R. Sun, Nat. Commun. **5**, 5554 (2014).
[48] Y. Li, S. J. Peng, T. T. Mao, D. J. Wang, K. M. Wu, J. R. Sun, and J. Zhang, AIP Adv. **7**, 055821 (2017).
[49] N. Shanthi and D. D. Sarma, Phys. Rev. B **57**, 2153 (1998).
[50] D. D. Cuong, B. Lee, K. M. Choi, H.-S. Ahn, S. Han, and J. Lee, Phys. Rev. Lett. **98**, 115503 (2007).
[51] C. Baeumer, C. Funck, A. Locatelli, T. O. Menteş, F. Genuzio, T. Heisig, F. Hensling, N. Raab, C. M. Schneider, S. Menzel, R. Waser, and R. Dittmann, Nano Lett. **19**, 54 (2019).
[52] S. Caprara, F. Peronaci, and M. Grilli, Phys. Rev. Lett. **109**, 196401 (2012).
[53] D. Bucheli, M. Grilli, F. Peronaci, G. Seibold, and S. Caprara, Phys. Rev. B **89**, 195448 (2014).